water

MDPI

Article

Hydrodynamic and Wave Responses During Storm Surges on the Southern Brazilian Coast: A Real-Time Forecast System

Arslaan Khalid [1,*], Andre de Souza de Lima [2], Felicio Cassalho [1], Tyler Miesse [1] and Celso Ferreira [1]

[1] Department of Civil, Environmental and Infrastructure Engineering, George Mason University, 4400 University Drive, Fairfax, VA 22030, USA; fcassalh@masonlive.gmu.edu (F.C.); tmiesse@masonlive.gmu.edu (T.M.); cferrei3@gmu.edu (C.F.)

[2] Centro de Filosofia e Ciências Humanas, Departamento de Geociências, Programa de Pós-Graduação em Geografia, Federal University of Santa Catarina, Campus Universitário, Trindade, Florianópolis, SC 88040-970, Brazil; geoandrelima@gmail.com

* Correspondence: akhalid6@masonlive.gmu.edu

Received: 24 October 2020; Accepted: 28 November 2020; Published: 2 December 2020

Abstract: Coastal flooding is a global phenomenon that results in severe economic losses, threatens lives, and impacts coastal communities worldwide. While recent developments in real-time flood forecasting systems provide crucial information to support coastal communities during coastal disasters, there remains a challenge to implement such systems in data-poor regions. This study demonstrates an operational real-time coupled surge wave guidance system for the coastal areas of Southern Brazil. This system is based on the recently developed integrated flood (iFLOOD) model, which utilizes the coupled hydrodynamic and phase-averaged ADCIRC–SWAN wave numerical model, driven by astronomical tides and atmospheric forcing from the Global Forecast System (GFS). This numerical modeling framework can simulate water levels and waves with a lead time of 84 h. A version of the coupled ADCIRC–SWAN model calibrated for Brazil, i.e., iFLOOD-Brazil, was operationally implemented (i.e., twice a day) over a period of 4 months (April to September 2020) for normal daily weather validation, as well as during a recent "bomb" cyclone that strongly impacted the southern coast of the country in June 2020. The real-time water levels and waves forecasted by iFLOOD-Brazil showed promising results against observations, with root mean square error (RMSE) values of 0.32 m and 0.68 m, respectively, for normal daily weather. Additionally, the RMSE values were 0.23 m for water levels and 1.55 m for waves during extreme weather, averaged over eight water level and two wave recording stations. In order to improve real-time predictions, a bias correction scheme was introduced and was shown to improve the water level and wave forecasts by removing the known systematic errors resulting from underestimation of astronomical tides and inadequate initial boundary conditions. The bias-corrected forecasts showed significant improvements in forecasted wave heights (0.47 m, 0.35 m) and water levels (0.17 m, 0.28 m) during daily and extreme weather conditions. The real-time iFLOOD-Brazil forecast system is the first step toward developing an accurate prediction model to support effective emergency management actions, storm mitigation, and planning in order to protect these economically valuable and socially vulnerable coastal areas.

Keywords: forecasting; iFLOOD; ADCIRC–SWAN; total water level

1. Introduction

Due to their relatively high frequency and intensity, coastal floods have long been considered to be among the most devastating natural hazards [1] on the planet, often resulting in the destruction

of coastal defenses and the consequential loss of lives and property [2]. These extreme events are the result of a series of non-linear interactions between meteorological and oceanographic drivers, including astronomical tides, wind-generated waves, and storm surges [3–5]. In addition, the severity of coastal floods is also dependent on the timing of the aforementioned processes [6]. For instance, if a storm surge lasts for more than half a day, it is likely to coincide with a high tide, potentially leading to greater coastal damages [7,8]. Lastly, the geometry of the coastal features, e.g., bays and estuaries, channels, and the width and slope of the continental shelf, exert a strong influence on the resulting total water levels [9,10]. Despite the evident complexity associated with the representation of the interactions between these mechanisms, it is well-known that the majority of deaths caused by coastal floods can be prevented with efficient emergency response strategies, improved planning, and accurate warning systems [11], which in turn intrinsically depend on timely and accurate flood forecasts [12]. In this context, a significant scientific effort has been made towards the development of reliable online real-time coastal flood forecast systems worldwide.

There are two methods used for real-time surge forecasts [13], namely (i) real-time simulations and (ii) pregenerated composite. Although often limited by the available computational resources, real-time simulations of flood forecasts using numerical models are preferred due to their real-time event-based characteristics [1,14]. In the last decade, several developed countries have benefited from the implementation of storm surge forecast systems. For instance, [15] developed a storm surge forecast system for the United Kingdom that has been operational since December 2009. This system was validated over 8 months, showing reliable predictions with an extended forecast of up to 7 days. Similarly, [16] proposed the Pan-European Storm Surge Forecasting System, which has shown satisfactory performance through most of the continent. Similarly, the Japanese Meteorological Agency (JMA) has provided a storm surge forecast since 2011, using 72-hour forecast time from the JMA's mesoscale atmospheric products, along with their depth-averaged shallow water model [17]. In the United States, a handful of regionally focused storm surge and wave forecast systems have been established for different parts of the country [11,13,18–22]. Finally, it is also worthwhile mentioning the platforms developed for South Korea [23] and Australia [24], which have also contributed to the mitigation of coastal flood hazards in these nations.

In contrast to developed countries, where losses due to coastal floods tend to have a more financial character (i.e., damage to property and infrastructure), emerging economies, especially those located in tropical and subtropical areas with low coastal plains and a broad continental shelf, usually also experience high death tolls during major storm surge events [25]. Therefore, current state-of-the-art studies have a focus on the implementation of operational coastal flood forecasts and warning systems in developing countries, which often lack proper coastal protection infrastructure, reliable bathymetric and hydrodynamic data, and efficient coastal hazard planning [26–28]. Rautenbach et al. [7] recently implemented a wind, wave, and storm surge forecast platform for South Africa, validating its results within acceptable ranges and successfully predicting particularly extreme storms. An operational early warning system for tropical cyclone inundation was also developed for the east coast of India, using the coupled advanced circulation (ADCIRC) and simulating waves nearshore (SWAN) models, providing surge forecasts with a 48 h lead time. In South America, a preoperational storm surge forecast–hindcast modeling system was presented by [29], encompassing most of the fast-flowing Rio de la Plata continental shelf between Argentina and Uruguay. In Brazil, [8] proposed a system of fully automated sea surface elevation, current, water temperature, and salinity forecasts focused on the Santos–Sao Vicente–Bertioga Estuarine System, focusing on navigation applications. Despite the innovation brought about by the aforementioned study, Brazil still lacks a reliable flood guidance system capable of fulfilling the emergency response and hazard planning demands of the country.

The southern coast of Brazil is constantly impacted by extreme surge events. The country is located near three major cyclogenesis regions [30]. On average, 108 extratropical cyclones are formed in the Atlantic Coast of South America every year [31]. According to [26], extratropical cyclones are the main storm surge driving mechanism in Southern Brazil. In a descriptive study, [32] observed

that from 1979 to 2008, a total of 40 major events (with wave heights above 6 m) impacted the region, leading to major coastal erosion and floods. These impacts may be aggravated, given that 40% of the Brazilian population (i.e., ~80 million people) lives within 60 km of the coast [33]. As a representative case of the aforementioned susceptible condition, the State of Santa Catarina, in Southern Brazil, is particularly vulnerable to storm surges. It is estimated that from 2000 to 2010, 17,000 people have been affected by such events in the state, with millions of dollars being lost in property damages; among the state's municipalities, Florianopolis, which is the state capital, is by far the most impacted city [34]. Once a country has a reliable coastal flood forecast system, decision makers can issue appropriate warnings, estimate potential damages, implement evacuation strategies, and manage emergency shelters [35,36]. However, such developments in Brazil are hampered by the alarming lack of in situ data [37] or the inexistence of a reliable flood forecast system.

In this context, the present study develops the first flood guidance system incorporating total water levels and waves in a user-friendly online platform for the coastal areas of Brazil (iFLOOD-Brazil, http://iflood.vse.gmu.edu/). The proposed system is based on the newly developed iFLOOD model [22], using the coupled 2D depth-integrated ADCIRC and SWAN phase-averaged spectral wave models, and forced by the Global Forecast System (GFS) [38]. Model calibration performed as a part of an earlier study by de Lima et al. [39] was used in this current forecast framework. This proposed framework was successfully validated during 4 months of daily weather (April to September 2020) and during the "bomb" cyclone of June 2020 against recently installed wave, meteorological, and water level gauges, accurately simulating tides, total water levels, and significant wave heights. In addition to the intrinsic challenge of implementing a state-of-the-art flood forecast framework in a poorly monitored area, this study presents a significant improvement to the forecast framework presented by [22] by means of a constantly updated bias correction strategy, named IFLOODv2. The efficacy of the bias-corrected iFLOOD-Brazil was demonstrated through its performance during the devastating bomb cyclone that hit Southern Brazil in June 2020. The 84-h lead time forecasts are freely available and provided every 12 h by iFLOOD-Brazil, having the potential to serve as a basis for emergency response and preparation throughout most of the South America Atlantic coast.

2. Materials and Methods

2.1. Study Area and Regional Meteorology

The study area encompasses the entire Southern Brazilian Shelf region, which extends from 22° S to 34° S (Figure 1). The region represents both the most susceptible areas to storm surges and the most densely populated coastal communities in Brazil. In these areas, storm surges can reach magnitudes of up to 2 m near the border with Uruguay, decreasing northwards and reaching approximately 1 m in the Rio de Janeiro State coastal areas [40]. A wide range of meteorological conditions, including frontal systems, medium- and upper-level cyclones, and mesoscale convective systems affect Southern Brazil [41]. These mechanisms often result not only in floods, but also in major wave generation, impacting coastal communities and offshore economical activities, such as navigation and oil exploration [30]. The potential losses to life and economy in Santa Catarina State may be aggravated due to its extensive and urbanized coastline, which lacks proper regional and urban planning policies, and due to its intense maritime port activity, which is responsible for 18 million tons of freight across five major ports throughout the state [26]. Storm surges between Argentina and Southern Brazil occur at periods of 6.5 to 11 days [26]. Furthermore, winds and atmospheric pressure gradients parallel to the coast generate surges that are usually propagated northward, having the same order of magnitude as the astronomical tides [26]. More than a half of these systems usually have a west-to-east track ranging between 28° S and 43° S, followed by almost 30% of events taking a southeast displacement (between 32° S and 57.5° S), both having cyclogenesis in the southern Uruguayan coast [32]. In addition to surge, major waves may also be generated on the southern or southeastern Brazilian coast due to cyclones. In an L-moments-based regional frequency analysis for the South Atlantic Ocean, [42] estimated 100-year

return period significant wave heights (Hs) of up to 9.5 and 6.5 m in the vicinities of South and Southeastern Brazil, respectively. However, the resulting impacts of such extreme events are strongly dependent on the topographic and bathymetric features of the affected region.

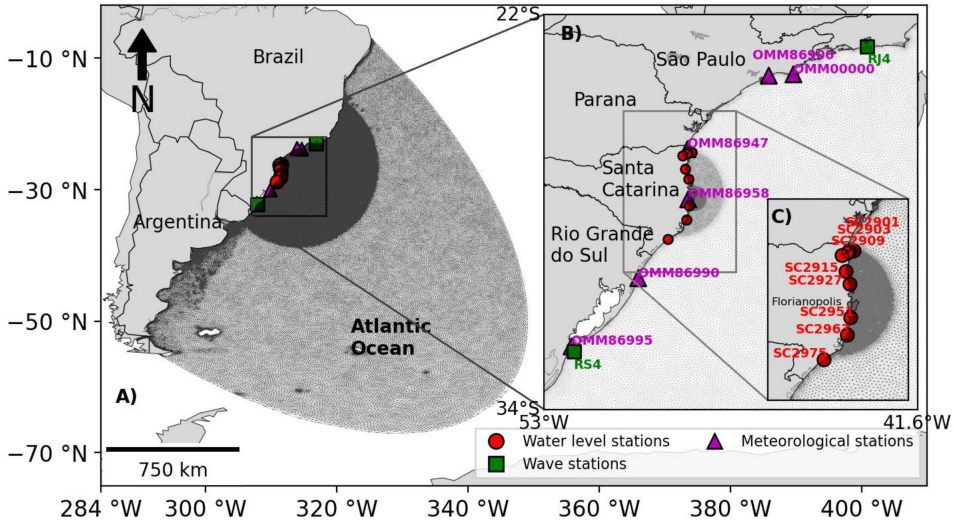

Figure 1. Location map of the study area. (**A**) Numerical modeling domain; (**B**) Southern Brazilian continental shelf region; (**C**) Santa Catarina state coastal areas.

2.2. Numerical Model and Setup

2.2.1. Coupled Hydrodynamic and Wave Model (ADCIRC–SWAN)

In this study, a coupled version of the hydrodynamic advanced circulation model (ADCIRC) and the simulating waves nearshore model (SWAN) is used [43]. The ADCIRC FORTRAN program is a finite-element hydrodynamic model based on the generalized wave continuity equation (GWCE) [44], which simulates the behavior of water levels and current velocities on an unstructured grid in space and time. The SWAN model is a third-generation phase-averaged wave model that simulates wave energy, propagation, and dissipation behaviors in open water bodies [45]. Detailed information on the governing equations of the ADCIRC and SWAN numerical models can be found in [43]. The coupled ADCIRC–SWAN model is used in several studies, with applications ranging from evaluating historical flooding [46–49] to forecasting future floods [20,21,49–52].

2.2.2. Numerical Mesh and Model Setup

The hydrodynamic numerical modeling domain for this study extends from 285° to 350° west and from 10° to 70° south, encompassing most of the South Atlantic Coast of Brazil. The unstructured computational grid was developed using the latest Matlab automated mesh generator, OceanMesh2D [53]. OceanMesh2D allows the construction of varying-resolution, project-specific, numerical meshes in the area of interest. The high-resolution coastline from the Global Self-Consistent, Hierarchical, High-Resolution Geography Database (GSHHG) [54] was used in the numerical grid. The semi-circular open ocean boundary was kept far away from the coastline to avoid boundary reflection and to include the effects of continental shelf processes. The horizontal mesh resolution in the modeling grid varies from 25 km in the open ocean to 30 m near Santa Catarina Island. The topography and bathymetry datasets were extracted from the General Bathymetric Chart of the Oceans [55] and local bathymetry survey datasets from the Brazilian Nautical Charts of the Brazilian Navy [54], with a vertical reference adjusted to the mean sea level (MSL) [56].

The coupled ADCIRC–SWAN model was configured to run in the explicit form of the barotropic setup. The semicircular ocean boundary of the model domain was forced by the amplitude and phase values of the 12 major constituents (M2, S2, O1, K1, K2, N2, Q1, M4, P1, 2N2, MS4, MN4) [57].

The harmonic analysis was performed by de Lima et al. [39] to analyze the accuracy of the modeled tides at three recordings stations (SC2927, SC2951, and SC2963) surrounding Santa Catarina by simulating the tides for 120 days in the year 2019 using 12 major constituents. A comparison of predicted tidal amplitudes against the observed constituents showed good agreement except for constituent S2 in all three recording stations, and except for constituents M4 and MS4 at SC2927 station. The RMSE values in the modeled total tidal amplitudes were 0.24, 0.1, and 0.11 m at SC2927, SC2951, and SC2963, respectively. Similarly, the predicted tidal phases of several constituents except M2 and S2 showed significant discrepancies against observed tidal phases. Since accurately modeling astronomical tides in real time is crucial for water level forecasting applications [22], these uncertainties in the predicted tides with this model lead to significant noise in the predicted total water levels. Therefore, we would expect a systematic bias when forecasting total water levels.

The atmospheric boundary forcing for the model simulations was provided by the National Centers for Environmental Prediction (NCEP) Global Forecast System (GFS). The GFS is a global spectral numerical model based on the primitive dynamical equations, which include a suite of parameterizations for atmospheric physics [38]. The GFS model provides global coverage of the forecasted parameters; in this study, 0.25-degree resolution (~24 km) is used to provide 10 m winds and sea level pressure (SLP) at 3 h outputs. The historical validation of total water levels and wave heights for three storms (2016, 2017, and 2019) described in [39] showed a reasonable agreement (RMSE values of 0.3 m for water levels and 0.71 m for wave heights) between predicted water levels and wave heights during the peak of the storm when forced by GFS atmospheric forcing. Although the European Centre for Medium-Range Weather Forecasts (ECMWF) weather model and Climate Forecast System (CFS) showed better validation in comparison to GFS, the unavailability of the forecasted products in real time voids its use for forecasting applications. This study, therefore, relied on the findings from the previously validated model results [39] based on the GFS wind model to forecast hydrodynamic and wave responses in real-time.

It is worthwhile mentioning that the computed wind stresses in nearshore areas are affected by the bottom friction imposed by different landcover classes [58]. The bottom friction parameterization influences the simulated hydrodynamic circulation and shallow-water wave energy, therefore Manning's n formulation in the ADCIRC model and Madsen's expression in the SWAN model are used to ensure accurate modeling. By definition, Manning's n, derived from the land cover type, is applied to all vertices in the numerical grid. Manning's n values are then translated to quadratic friction coefficients by ADCIRC and are used in the bottom stress calculation and free surface shear stress [58]. The landcover types are extracted based on the global dataset from the Copernicus land monitoring service and attributes for wind reduction due to local tree canopy and directional wind roughness are incorporated into the modeling set up as well. These wind reduction attributes help simulate accurate estimates of transferred momentum, which in various studies [47,59–61] is shown to improve the accuracy of simulated storm surges. Wetting and drying, non-linear bottom friction, advection, finite-amplitude terms, convective acceleration, and the time derivative of convective acceleration were included in the simulations.

2.3. iFLOOD Operational Workflow

The schematic workflow for iFLOOD flood forecasts in Brazilian coastal areas is presented in Figure 2. The flood forecast operation starts by retrieving the atmospheric forcing from the NCEP National Oceanic and Atmospheric Agency (NOAA) file transfer protocol (ftp) portal. These GFS atmospheric model files are uploaded every 6 h at 00Z, 06Z, 12Z, and 18Z h for a lead time of 84 h. We downloaded the raw files at 06Z h and preprocessed them using the wgrib utility provided by NCEP to manipulate GRIdded Binary (GRIB) files, which extracts the 10 m wind and sea level pressure values and regrid variables from lambert conic conformal (LCC) and geographic (GCS) projection data. A set of Network Common Data Form (NetCDF) commands in the Python script then extracts the regrided data and writes in a text format for direct input into the ADCIRC model. Modeled static input files containing

the numerical mesh and attribute file are often updated during a major forecast system revision process, while the model control file is updated every forecast cycle using Python scripts. Each forecast cycle is initialized by a hotstart file generated using the short-term forecast cycle. The model control file consisting of tidal boundary information is only updated if the forecast system needs to be restarted. A detailed description of the restart (hindcast), short-term forecast, and forecast cycle can be found in [22]. The coupled ADCIRC–SWAN simulation is implemented on a 32-core dedicated Linux Server at the Mason Flood Hazards Research Lab. The ADCIRC–SWAN model simulates the forecasted water level, current, and wave parameters based on the tidal boundary, initial boundary conditions, and forecasted wind and pressure fields from GFS models. The model takes nearly 1 h to complete the 84 h of forecast simulation. The NetCDF model outputs are further processed into various data formats (GeoJSON, ESRI Shapefile, KML, text files, etc.) using a set of Python and bash routines. This process takes an additional 10 min and the final processed model results, along with real-time observations, are freely available on the iFLOOD web portal (https://iflood.vse.gmu.edu/).

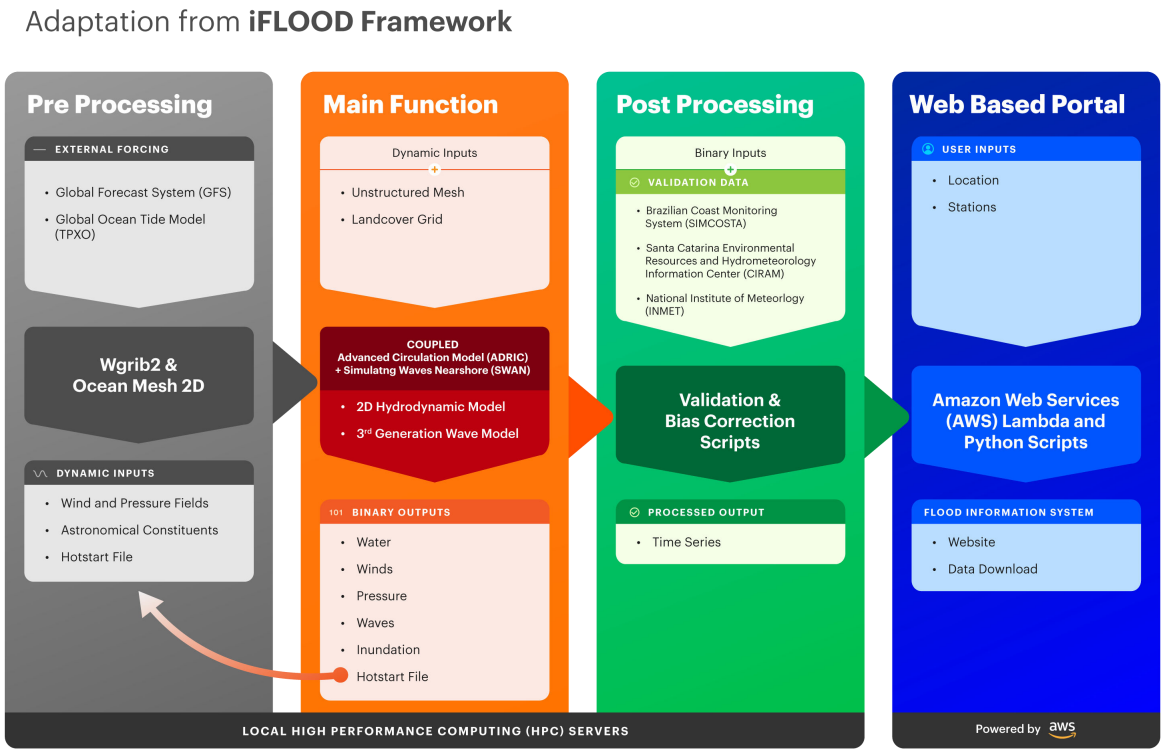

Figure 2. Operationalization framework for integrated flood for Brazil (iFLOOD-Brazil) model.

2.4. Data

Six meteorological stations of the National Institute of Meteorology (INMET) were selected along the study area for wind and pressure validation. The meteorological stations have wind recordings at different vertical heights, which are converted to 10 m height wind speeds using an empirical formulation described by Fleming et al. [50]. Additionally, two deep-ocean wave recording stations were also used to validate wind measurements. Currently, only two buoys maintained by the Brazilian Coast Monitoring System (SIMCOSTA) are operational for real-time wave observation in Southern Brazil, which were, therefore, selected for our model validation. In addition to the wave forecasts from the iFLOOD-Brazil system, WAVEWATCHIII [23,52,60] (WW3) is the only wave forecast system that runs on a global domain encompassing the South Atlantic Ocean, where it provides guidance on ocean swells and wave spectra. The wind waves provided by the global WW3 system were compared to the iFLOOD wind waves for comparison of the forecasted data.

In addition, eight tide gauges maintained by the Santa Catarina Environmental Resources and Hydrometeorology Information Center (Epagri/CIRAM) were selected for water level validation, in which the measurements were converted from local vertical data to mean sea level (MSL) values. Although a large number of tide gauges are available, they are mostly located along the coast of Santa Catarina State only. A post-bias correction scheme similar to iFLOOD and ETSS [22,61] was used to minimize the systematic water level and wave forecast errors for each station. The systematic error in the current modeling framework can result from inaccurate astronomical tides, inadequate initial boundary conditions, missing wave run up information, wind forcing errors, omitting flooding from rain data, omitting sea level rises, and model bias [62]. The correction value for the post-bias correction scheme was calculated based on the raw bias between the predictions and observed data at the recording station for the first 4 h of the latest forecasts. This was then applied as a correction to the latest water level and wave forecasts using Equation (1) for each forecast advisory. Contrary to water level and wave forecasts, bias-corrected (iFLOOD) wind model outputs were not generated, since GFS fields are grid-based, and thus require a large number of observation stations.

$$\text{iFLOODv2} = \text{raw iFLOOD model outputs} \pm \text{correction value} \quad (1)$$

Although the coastline of Brazil is highly vulnerable to storm surges and waves, limited observational data are available [39]. Figure 1 shows the available network of real-time meteoceanographic observational data stations that was employed for model validation in our research. This included eight water level, six meteorological, and two wave recording stations, shown in Figure 1 as red circles, magenta triangles, and green squares, respectively.

2.5. Case Studies

2.5.1. Daily Weather (April to August 2020)

The iFLOOD-Brazil model's performance was evaluated based on forecasted water levels, waves, and winds from the ADCIRC–SWAN coupled system, which were produced twice a day for four (4) consecutive months in 2020 (26 April to 2 September 2020). During this period, one week of iFLOOD forecast information (28 June to 5 July 2020) for the bomb cyclone (discussed in Section 2.5.2) was removed in order to evaluate the iFLOOD-Brazil model's performance under normal weather conditions. These iFLOOD forecasts were assessed by comparing the model results against observations from the recording stations. A detailed description of the recording stations used for the daily weather forecasts is available in Table 1.

Table 1. List of recording stations used in the case studies.

Station Full Name	Station ID	Longitude	Latitude
Bertioga-A765	OM86900	−46.14	−23.84
Itapoa-A851	OMM86947	−48.64	−26.08
Florianopolis–Sao Jose-A806	OMM86958	−48.62	−27.60
Tramandai-A834	OMM86990	−50.14	−30.01
Rio Grande-A802	OMM86995	−52.17	−32.08
Ilhabela	OMM00000	−45.40	−23.81
RS-4	RS4	−52.09	−32.25
RJ-4	RJ4	−43.15	−22.97
Ilha da Paz (SFS)	SC2901	−48.49	−26.18
Itapoa—Porto Itapoa	SC2903	−48.60	−26.19
Sao Francisco do Sul—TESC I	SC2909	−48.64	−26.23
Barra Velha (Itajuba)	SC2915	−48.68	−26.69
Balneario Camboriu—Praia de Laranjeiras	SC2927	−48.59	−26.99
Florianopolis—Caieira I	SC2951	−48.56	−27.81
Imbituba—Porto de Imbituba	SC2963	−48.65	−28.23
Balneario Rincao—Plataforma de Pesca	SC2975	−49.21	−28.83

SFS—Sao Francisco do Sul; TESC I—Terminal Santa Catarina.

2.5.2. Bomb Cyclone Case Study (June 2020)

The cyclone in question emerged as an extratropical system with low atmospheric pressure from the Atlantic Ocean. This type of system is known as a "bomb" cyclone, characterized by a sharp drop in atmospheric pressure over a period of 24 h [63]. The bomb cyclone occurred on 30 June 2020, bringing winds of over 33.3 m per second (120 kph), which prompted coastal flood warnings in Santa Catarina as a result of major storm surges [63]. Extensive rainfall measuring 140 mm in 24 h increased the water levels above flood levels in some areas of Rio Grande do Sul. In total, more than 10 people died and 686,000 thousand people were left without electricity or basic supplies [63]. The iFLOOD-Brazil forecast system was operational during this bomb cyclone and predicted the water level and waves at a number of recording stations. Figure 3 shows the forecasted wind (magnitude and direction) and pressure values from the GFS model at a forecast initialization time of 06Z UTC during the passage of the cyclone. It can be clearly seen that the GFS model predicted a massive cyclone system going over Florianopolis Island, with forecasted winds of 10 to 15 m/s and atmospheric pressure dropping to 1000 mb on 30 June 2020. The meteorological recording station, Florianopolis–Sao Jose-A806 (OMM86958), recorded the highest wind speeds of 7.4 m/s at 5 m height (approximate 10 m height wind speeds of 9.12 m/s) and the lowest atmospheric pressure of 996.7 mb on 30 June 2020.

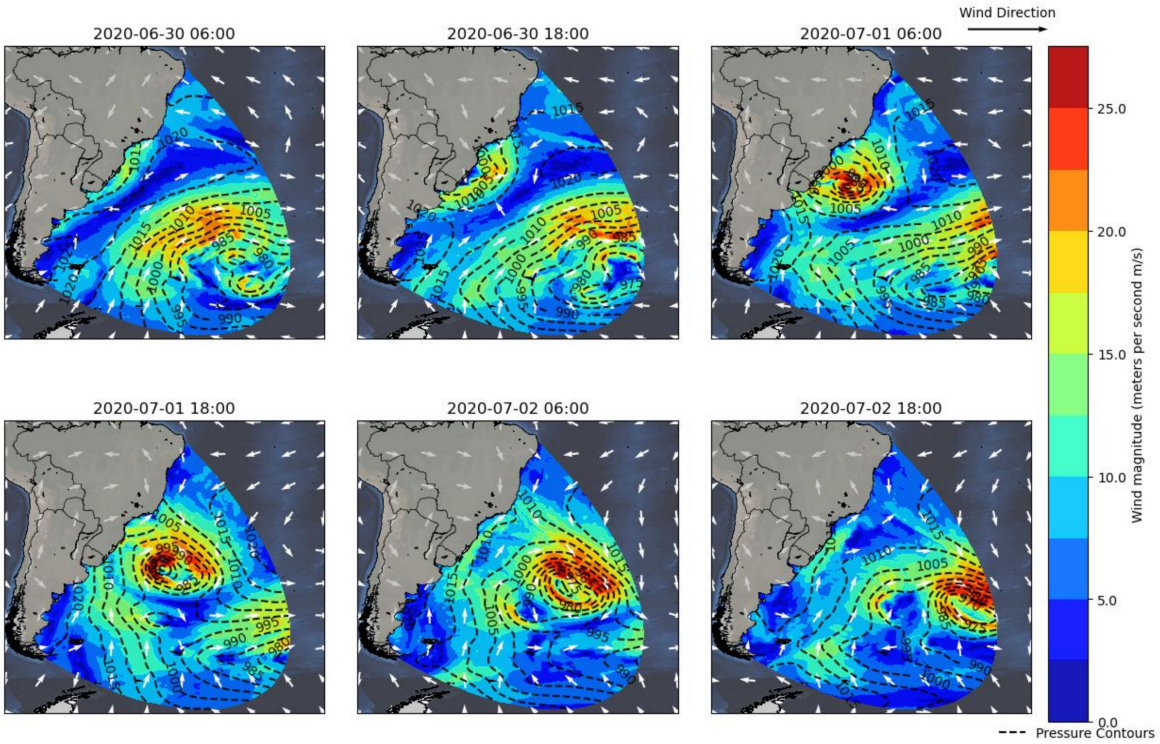

Figure 3. Global Forecast System-model-forecasted wind and pressure fields for the bomb cyclone (2020) at 06Z UTC on 30 June 2020.

2.6. Verification Metrics

Bias, root mean square error (RMSE), R-square coefficient (R2), and Pearson correlation coefficient (r) metrics were used for model verification. The mean absolute error (MAE) represents the average offset in the model predictions against the observations. The RMSE represents the square root of the difference between prediction and observation datasets. The R2 coefficient represent the square of the correlation coefficient. The Pearson correlation coefficient (r) measures the linear correlation between the predictions and the observations. The values of "r" are usually between −1 and 1. The validation of the iFLOOD-forecasted water levels, wave heights, and wind speeds was accomplished by comparing

the forecasted variables against observations at recording stations. The equations for these verification metrics are as follows:

$$\text{Bias} = \frac{1}{N}\sum_{i=1}^{N}(P_i - O_i)^2 \quad (2)$$

$$\text{RMSE} = \sqrt{\frac{\sum_{i=1}^{N}(P_i - O_i)^2}{N}} \quad (3)$$

$$\text{R}^2 = 1 - \frac{RSS}{TSS} \quad (4)$$

$$\text{MAE} = \frac{\sum_{i=1}^{n}|P_i - O_i|}{n} \quad (5)$$

$$r = \frac{\sum_i (O_i - O_{im})(P_i - P_{im})}{\sqrt{\sum_i (O_i - O_{im})^2 \cdot \sum_i (P_i - P_{im})^2}} \quad (6)$$

where *Oi* represents the observations and *Pi* represents the predicted values from the model, whereas *i* is the time interval and *N* is the total number of datasets. *Oim* and *Pim* are the means of the observed and predicted values, respectively. *RSS* and *TSS* represent the sum of the squares of the residuals and the total sum of the squares, respectively. Additionally, all of the verification metrics values obtained at each recording station were averaged, taking into account all of the forecast advisories.

3. Results and Discussion

3.1. Daily Evaluation

Figure 4 presents a scatter plot of the wind speeds calculated by iFLOOD (after interpolation and drag modifications of the GFS wind forecast) from the coupled ADCIRC–SWAN numerical model compared with interpolated wind measurements at eight monitoring stations based on a height of 10 m. The GFS operational winds driving the iFLOOD values showed overall good agreement with the observations from all recording stations, except for OM86990. The scatter plot of the predicted and observed wind speeds shows that the wind forecast RMSE values ranged between 1.28 and 4.41 m/s. The wave recording station, RJ4, in the deep water had the highest RMSE (4.41 m/s). Additionally, station RJ4, showed consistent underprediction of wind speeds. Several studies have suggested that limited observational data in the southern hemisphere leads to underestimation of wind speeds at some locations [64,65].

The highest water levels measured at all the eight recording stations (Figure 1) during each forecast advisory were compared against the water levels peak predicted by iFLOOD (Figure 5) and the bias-corrected forecasts (iFLOODv2). The scatter plots show that the predicted peaks for total water levels from iFLOOD and iFLOODv2 models generally matched well (closer to the equal line) with the observations; however, the current modeling setup showed a tendency to underestimate the predicted peaks of total water levels at all stations. The average RMSE values varied from 0.2 m to 0.43 m for iFLOOD over the period of 4 months, while the RMSE values were reduced to a range of 0.2 m to 0.36 m for the bias-corrected forecasts (iFLOODv2). Analysis of the predicted water levels suggests that the inherited tidal error and missing M3 constituent [39,66] results in larger RMSE values for stations SC2901 to SC2915, even after using bias-corrected forecasts (iFLOODv2). Stations SC2927 to SC2975 showed a significant improvement in the maximum water level predictions (scatter moves closer to the equal line) using the bias-corrected iFLOODv2 forecasts, suggesting that the systematic bias observed at these stations was successfully removed. In terms of peak timing, visual inspection of time series data at stations SC2901 to SC2915 showed a phase shift every 7–14 days, leading to a timing offset of nearly 4 h between predictions and observations. This timing offset in the water level peaks was likely the result of the N2 tidal phase not being correctly modeled, as well as being affected by the missing M3 tidal constituent [39] at the

station North of Florianopolis, SC2951 (SC2927 to SC2901). The peak timing for modeled and observed water levels at stations SC2951 to SC2975 matched correctly (within one hour), which is consistent with the lower RMSE values for predicted iFLOODv2 water levels.

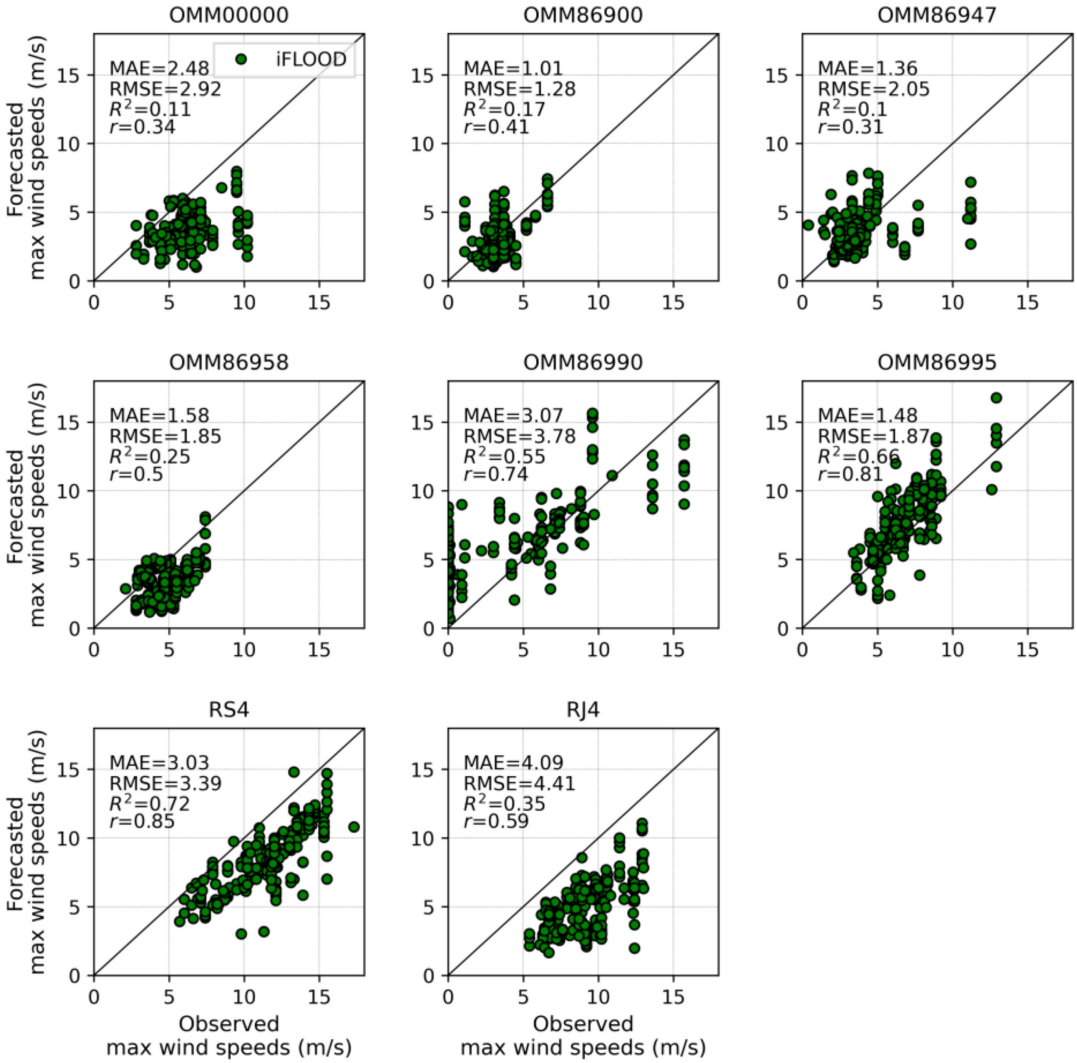

Figure 4. Scatter plots of predicted maximum wind magnitudes vs. observed peak speeds at 6 meteorological stations and 2 wave recording stations under daily weather conditions from 26 April to 31 August 2020. The mean absolute error (MAE), root mean square error (RMSE), R-square coefficient (R2), and Pearson correlation coefficient (r) metrics are shown in each subplot.

The scatter plot comparing the peaks of wave heights forecasted by iFLOOD and iFLOODv2 models against the observed datasets shows good agreement (closer to line) for recording station RS4 but a large underestimation for RJ4 in Figure 6. The RMSE for the predicted wave heights at RJ4 station using iFLOOD raw model outputs gave a value of 1.02 m, which was reduced to 0.61 m using bias-corrected model outputs (i.e., iFLOODv2). A consistent underestimation of the wind speeds resulting in the highest RMSE (4.41 m/s) value being observed at RJ4 could be directly responsible for the underestimation of wave heights. Furthermore, inconsistent bathymetry depths at the RJ4 station in the model (6.5 m compared to 18 m) could have resulted in smaller wave heights.

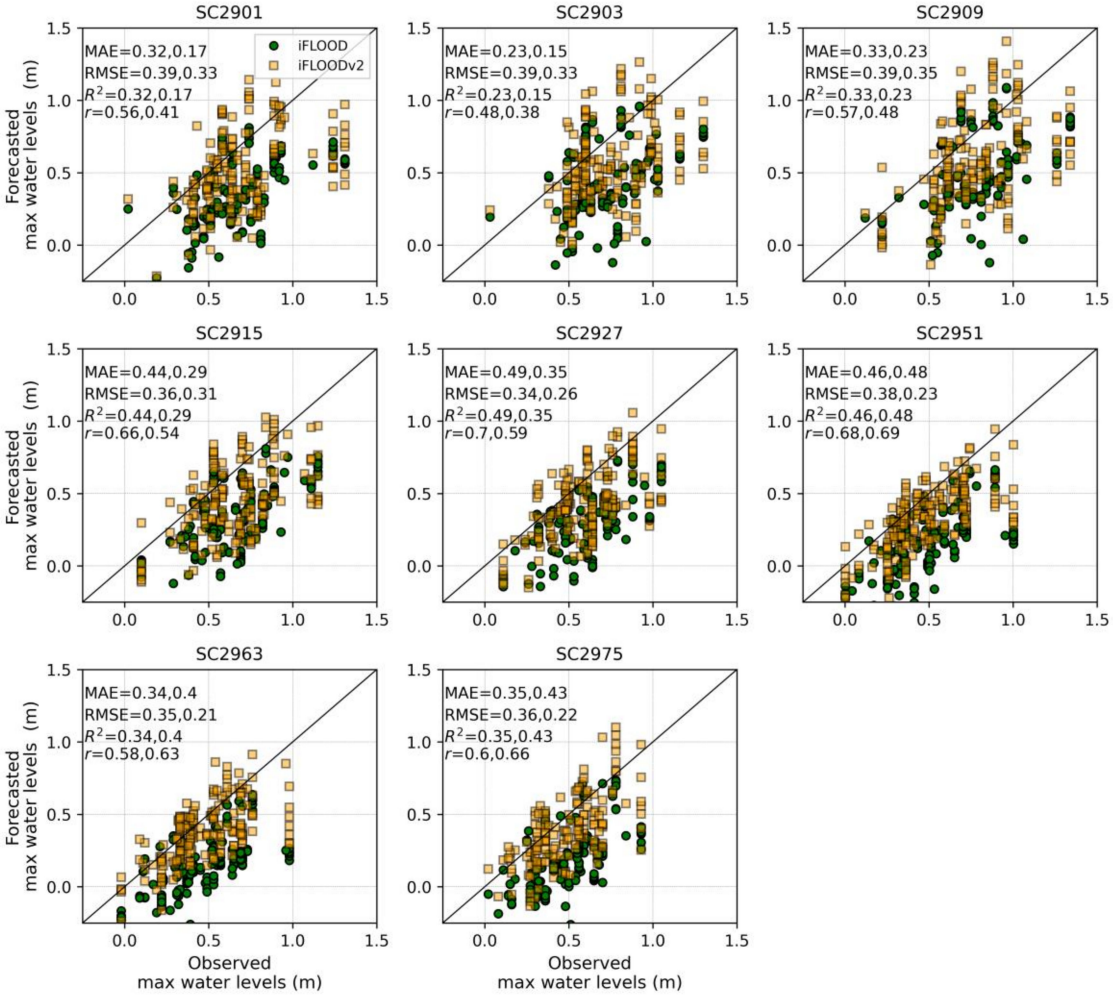

Figure 5. Scatter plots of predicted peaks of total water levels vs. observed peaks under daily weather conditions from 26 April to 31 August 2020.

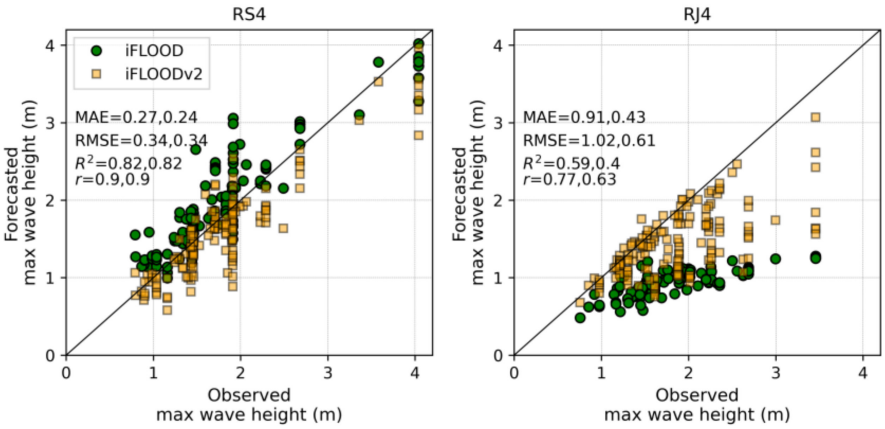

Figure 6. Scatter plots of the predicted maximum significant wave heights vs. observed waves during daily weather conditions from 26 April to 31 August 2020.

3.2. Extreme Weather Evaluation

The forecasted wind speeds from the GFS model were compared at eight recording stations (Figure 1) from 28 June to 2 July 2020, and peak bias is shown as a bar plot in Figure 7. The forecast

advisories issued several days in advance (−F05 to −F01) leading to the last forecast before the peak of the storm (F00) showed varying levels of bias for all recording stations. Most of the recording stations showed an underprediction of wind speeds, except OMM86990 and OMM86995. The overestimation of winds at these 2 recording stations (OMM86990 and OMM86995) could have resulted from the absence of wind reduction features (such as buildings, trees, etc.) not included in the current modeling domain extents (limited to coastline features). The underprediction of maximum wind speeds resulted in a direct underestimation of maximum water levels and wave heights.

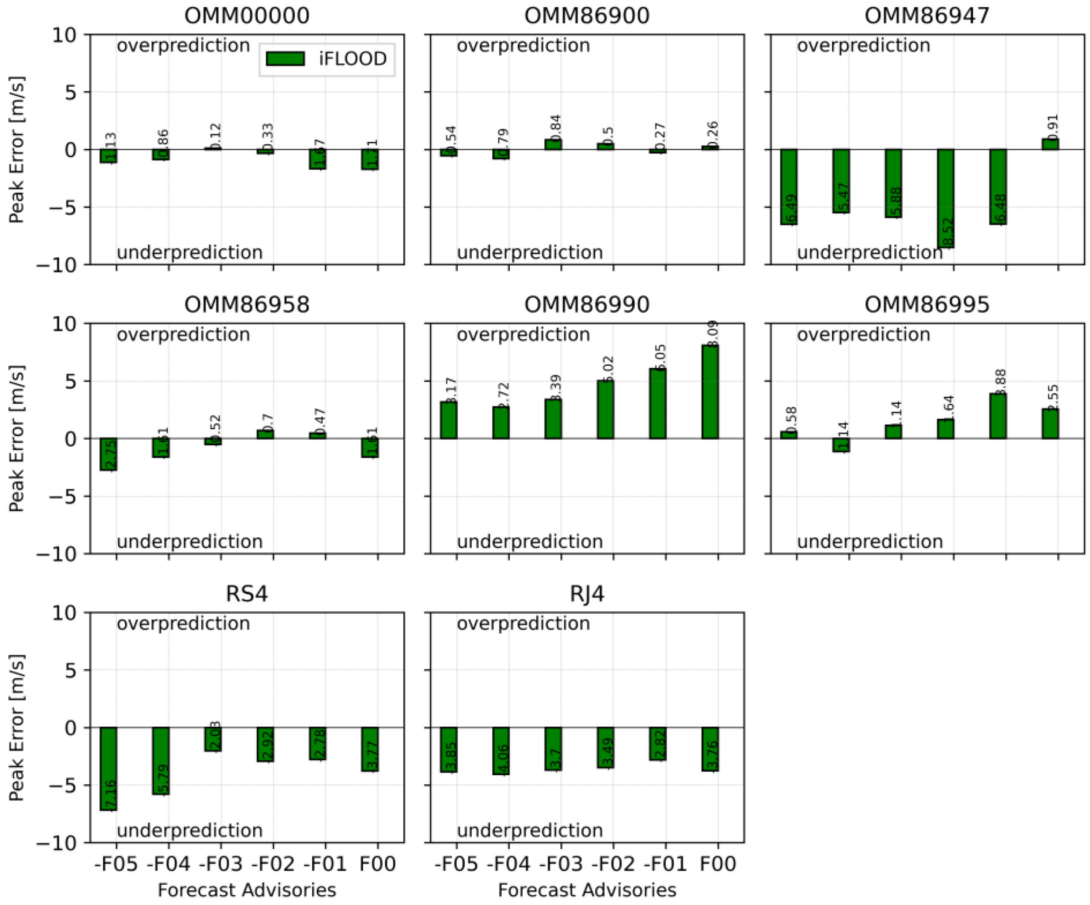

Figure 7. Bar plots of peak errors for forecasted maximum wind speeds (10 m height) at 6 meteorological stations and 2 wave recording stations during the bomb cyclone of 2020. F00 represents the forecast advisory on 1 July at 18:00 UTC, while the bars before F00 represent the forecasts issued earlier at 12 h intervals.

The time series plot in Figure 8 shows the forecasted total water levels at all recording stations from 28 June to 5 July 2020. The bomb-cyclone-induced storm surges increased the total water levels to almost 1 m above MSL at three recording stations (SC2901 to SC2909). The forecasted water levels in Figure 8 also show consistently high water levels based on the iFLOOD-Brazil forecasts prior to the storm. Upon analysis of the peak bias, we noticed an underestimation of almost 0.1 m averaged over all stations during the peak maximum water levels. Here, iFLOODv2 forecasts showed similar predictions as iFLOOD, except on 1 July at 18:00 UTC, where the predicted maximum water levels matched the observed water levels at almost 1 day lead time.

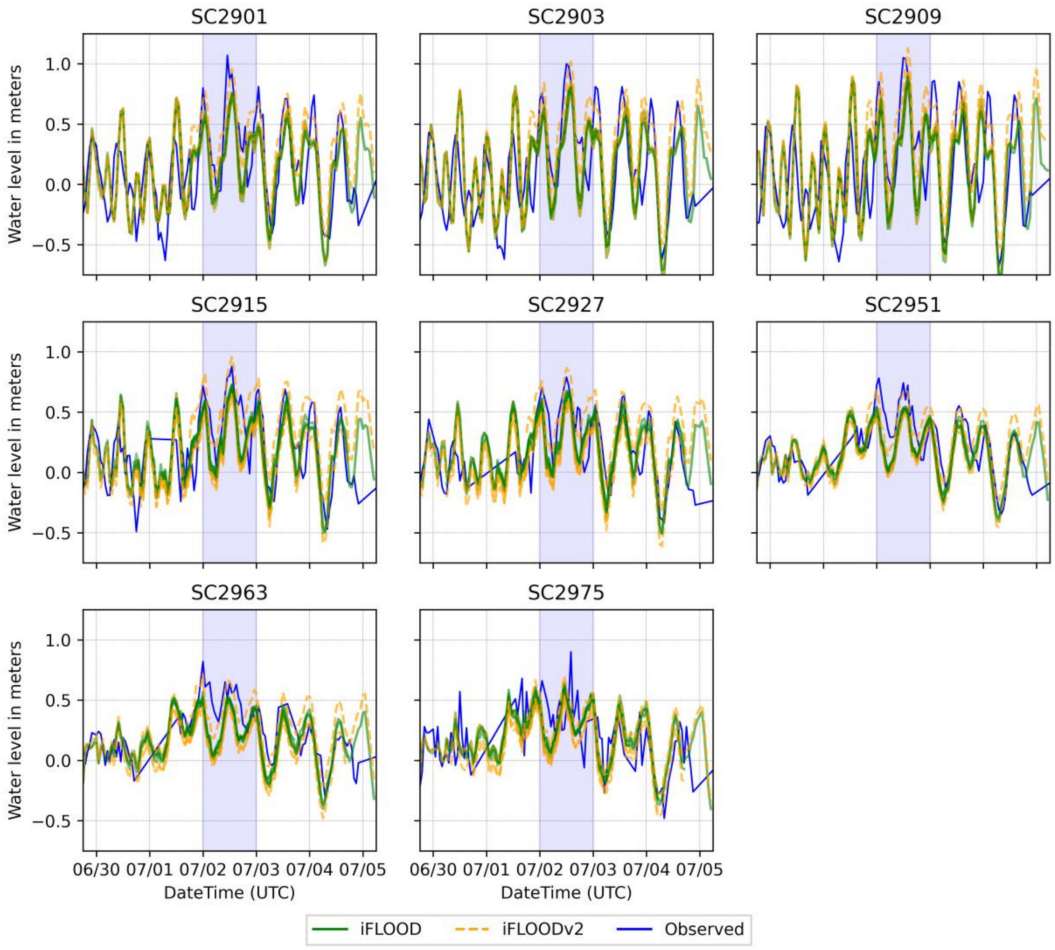

Figure 8. Time series plots of total water level forecasts compared against the observations, issued during the bomb cyclone between 28 June and 2 July 2020. The shaded gray vertical area shows the peak of the storm.

The forecasted peaks of the water levels at all the eight recording stations were further compared against the observed peaks and computed peak bias (predicted peak minus observed peak) during the forecasts issued between 28 June and 2 July 2020, and are shown as a bar plot in Figure 9. The bar plot for iFLOOD water level forecasts suggests that the framework is capable of predicting water levels nearly 5 advisories in advance (2.5 days lead time), with an average bias of 0.23 m for stations SC2901 to SC2975. The bar plots for various stations also show that the iFLOOD forecasts did not steadily improve as the lead time diminished; instead, a somewhat constant bias can be noticed. The iFLOODv2 forecasts, on the contrary, show an increase in bias (average bias of 0.29 m for all stations) leading to storm day (F00), suggesting that there was no additional improvement by using bias-corrected water level forecasts during the extreme weather (bomb cyclone).

The bar plot of the forecast error for the maximum wave heights predicted by iFLOOD (Figure 10) for RS4 shows a steady decreasing trend for forecasts leading to the storm. Station RJ4, on the contrary, showed a consistent underprediction, which was similar to the daily forecasts. Bias-corrected forecasts (iFLOODv2) showed an advantage over iFLOOD at both stations, however the bias increased for forecasts leading up to the storm. In order to provide an estimate of the forecasted wind waves modeled in the iFLOOD domain to other modeled wind waves, we compared the wind waves forecasted from the WW3 system at two recording stations. The significant wave heights of the wind waves from the forecast systems was compared to the observations to calculate and compare the bias (shown in Figure 10). The absence of bar plots for WW3 forecasts earlier than F03 was due to issues during the preprocessing phase of the WW3 data. WW3 forecasts retrieved for evaluation against the observations

during the storm showed the smallest error for RJ4, however the average forecast error was almost the same as for iFLOODv2 for RS4. The underprediction of wind speeds and shallower bathymetry at station RJ4 was directly shown to affect the accuracy of the forecasted significant wave heights for this station.

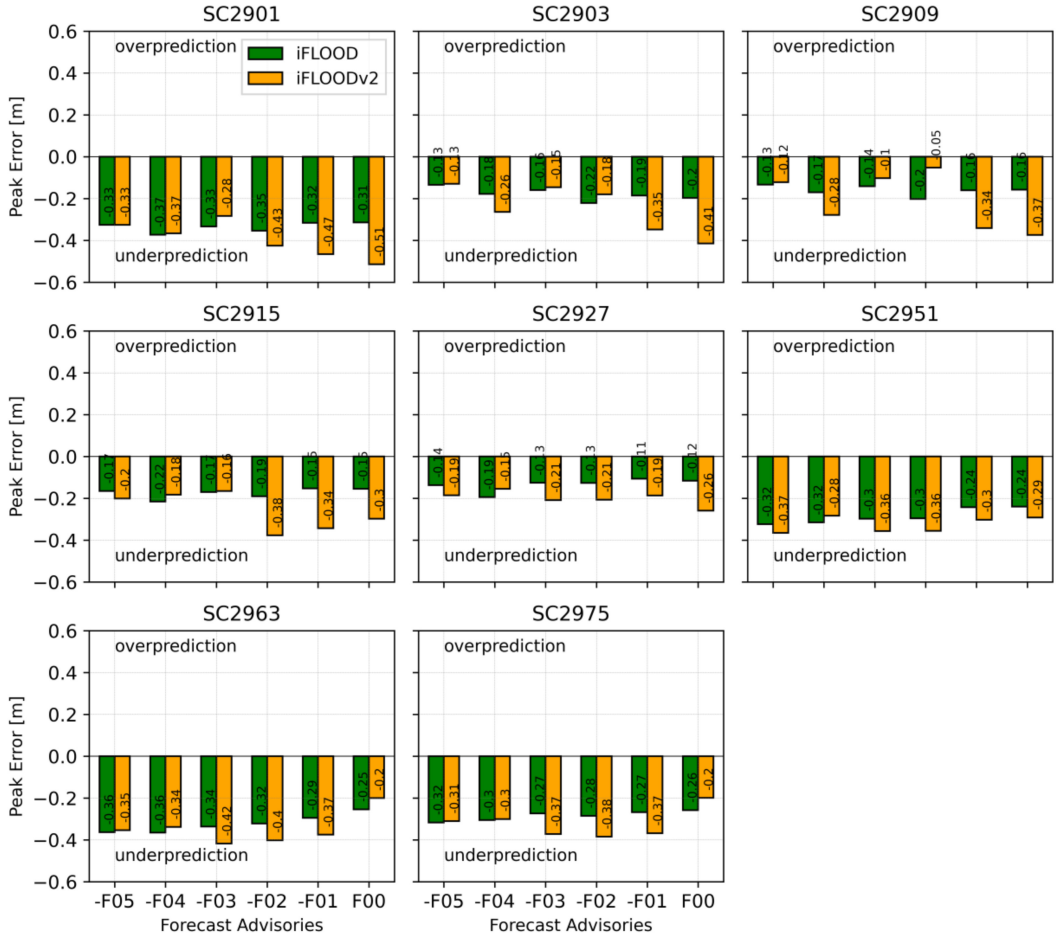

Figure 9. Bar plots of peak errors for maximum water levels at 8 wave recording stations during the bomb cyclone of 2020. F00 represents the forecast advisory on 1 July at 18:00 UTC, while the bars before F00 represent the forecasts issued earlier at 12 h intervals.

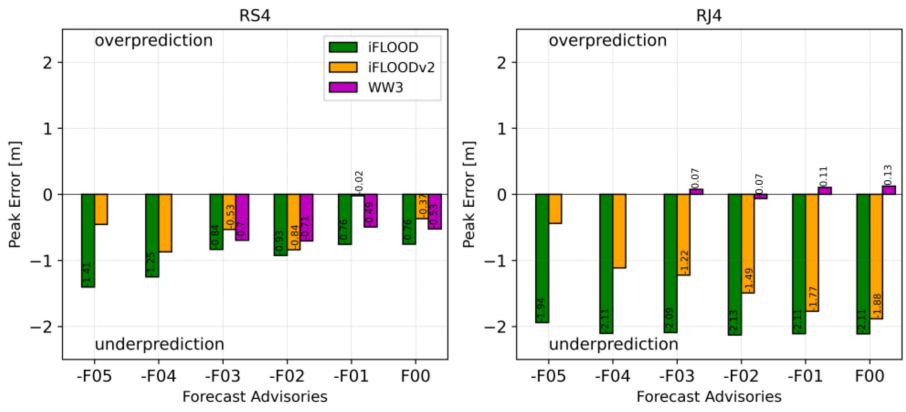

Figure 10. Bar plots of peak errors for maximum wave heights at 3 wave recording stations during the bomb cyclone of 2020. F00 represents the forecast advisory on 1 July at 18:00 UTC, while the bars before F00 represent the forecasts issued earlier at 12 h intervals.

The spatial distribution of the computed RMSE values for the forecasted winds, water levels, and waves from iFLOOD and bias-corrected (iFLOODv2) models during daily and extreme weather conditions is shown in Figure 11. In the spatial map, RMSE values for iFLOOD are shown in the range of 0.1–0.5 m, which were reduced to a maximum of 0.35 m using iFLOODv2 during daily weather conditions. For extreme weather, certain color tones (yellow to red) show higher RMSE values at several stations when using iFLOODv2 in comparison to iFLOOD. On the contrary, the RMSE values at both wave recording stations were clearly lowered using iFLOODv2 forecasts in comparison to iFLOOD for both weather conditions. Figure 11 also shows that the RMSE values for wind and wave forecasts were almost the same under daily and extreme weather conditions, except at certain stations.

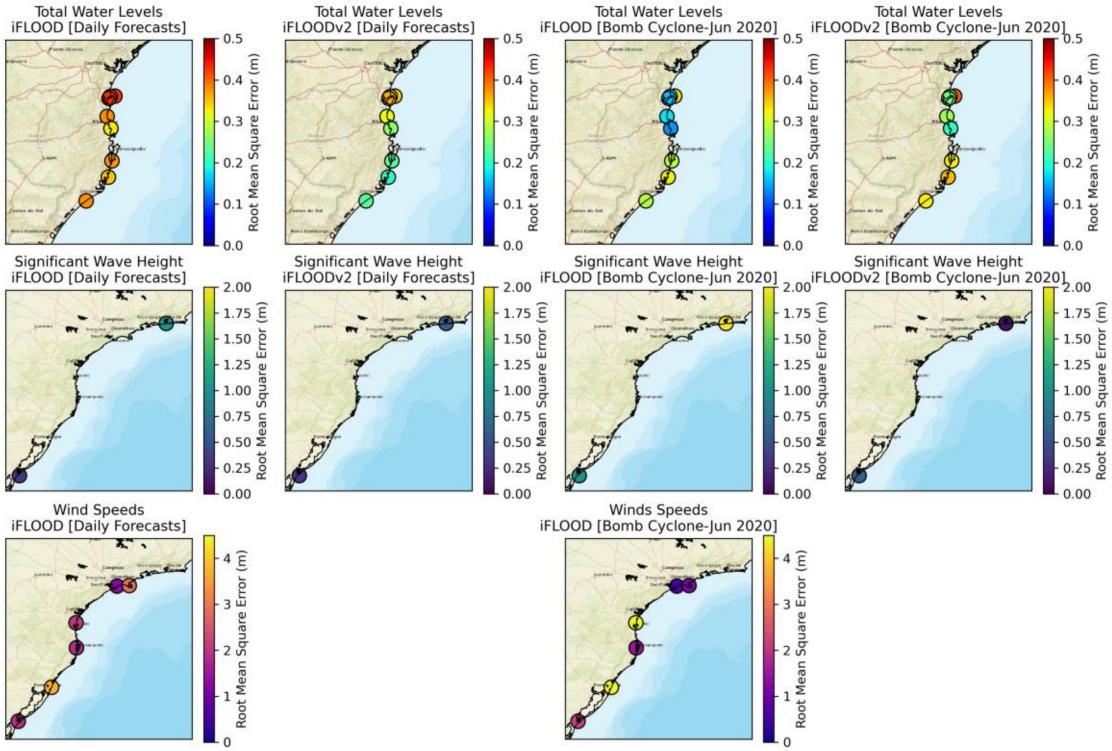

Figure 11. Spatial distribution of the computed RMSE values for forecasted products from iFLOOD and bias-corrected iFLOODv2 models at various recording stations during daily and extreme weather in 2020.

The accuracy of the simulated hydrodynamics and waves inside the computational modeling domain was dependent on the accuracy of the meteorological forcing [67], which was GFS in this case. A previous [39] study showed that the GFS weather model was able to perform reasonably well with underpredictions (RMSE values of 0.3 m and 0.7 m for water levels and waves) in terms of estimating the historical peak water levels and significant wave heights. Our model validation for daily and extreme weather forecasts also shows that real-time meteorological forcing from GFS has a similar tendency to underpredict the wind speeds, which is translated into underestimation of predicted water levels and significant wave heights. Various studies also showed the use of a constant correction factor to improve the accuracy of wind and pressure fields [68,69]. On studied [70] argued that the horizontal resolution of the weather models also plays an important role in the accuracy of the surface winds; for instance, coarser-resolution wind models tend to underestimate maximum wind speeds [61]. Here, we used a 0.25-degree horizontal resolution, which might be partially responsible for the underestimation of winds.

Besides the accuracy of the atmospheric forcing, astronomical tide modeling also plays a crucial role in estimating total water levels. Due to the complex nature of the tides in the study area and the limited availability of forced tidal constituents [39], a systematic error was present in the modeled

astronomical tides, leading to underestimation of total water levels. Bias-corrected schemes [71] are often applied in operational flood modeling frameworks to improve the accuracy of forecasted products. Here, we applied a similar approach for the total water level and wave forecasting, and found a clear improvement in accuracy during the daily weather forecasts. However, the same bias correction scheme showed no additional value during the extreme weather forecasts (bomb cyclone). The authors believe that bias-corrected forecasts (iFLOODv2) worked well during daily weather, since they were beneficial in removing the known systematic errors from modeled tides, while in extreme weather the errors might not be systematic, but instead could be due to missing physical processes (baroclinic processes, inaccurate winds, etc.) [72]. These physical processes require a 3-D framework to be established, which significantly increases the computational cost, making the model highly inefficient for real-time operations. However, various studies [73–78] have stressed the importance of using 3-D frameworks to improve forecast accuracy.

Wind-driven forces represent a major part of the significant wave heights generated locally [43]. Additionally, these wind-driven waves are known to affect the water levels near shore, which can increase by 5–20% on broad continental shelves and by as much as 35% on steep slopes [43]. Therefore, a coupled hydrodynamic and wave modeling approach was used to improve the accuracy of the modeled water levels, and additionally to simulate waves using the same computational grid in the study. In our comparison, iFLOODv2-forecasted wave heights showed same accuracy as WW3 at RJ4, however showed lower accuracy at RS4 during the bomb cyclone, which is believed to been caused by consistent underprediction of wind speeds. One study [79] involving extensive experimentation also showed that improvements in wave forecasts are directly related to higher quality surface winds. Even though iFLOOD and WW3 used the same GFS weather model, both systems forecasted quite different wave heights. The higher accuracy of the wave forecasts by WW3 could result from data assimilation, a technique that is not yet implemented in the iFLOOD-Brazil forecast system. Such data assimilation serves as a bias correction method for imperfect numerical schemes and approximated physical processes within models to optimally improve wave predictions [80]. Therefore, to improve the current performance of iFLOOD-Brazil forecasted outputs, these limitations should be incorporated within the modeling framework.

4. Conclusions

This study assessed a framework for forecasting of hydrodynamic and wave conditions in the coastal areas of Southern Brazil. This framework was based on the fully coupled ADCIRC–SWAN surge wave model, which was set up in the South Atlantic Ocean to provide total water level and wave forecasts with a lead time of 84 h using the GFS weather model. The iFLOOD-Brazil forecast system was developed to aid coastal emergency managers in developing real-time flood forecasts. This system has been operational since April 2020, and the forecasts generated in real-time were compared against observations to evaluate its forecasting performance. The evaluation period consisted of four consecutive months of daily weather performance data, as well as the bomb cyclone event that occurred in June 2020 to provide extreme weather forecasting data.

Average underestimation of wind forcing (2.23 m/s, 2.27 m/s) was noted during both case studies (daily, extreme), which resulted in underprediction of maximum water levels (0.32 m, 0.23 m) and significant wave heights (0.68 m, 1.55 m). Bias-corrected forecasts from iFLOODv2 showed improvements in the forecasted products for water levels (0.17 m, 0.28 m) and wave heights (0.47 m, 0.35 m) during normal weather conditions only. These iFLOODv2 forecasts were shown to improve the predicted hydrodynamic and wave results at the recording stations by removing a known systematic error, while during extreme weather events no additional value was added. On average, the maximum forecasted heights for the water level and wave height were predicted 2.5 days in advance. However, some limitations that may have influenced the forecasting accuracy of iFLOOD should be highlighted. First, the underestimation of the water levels while modeling astronomical tides, which result from the complex nature of the governing tidal constituents (i.e., missing constituents in the tidal prediction

models), must be noted. The second and most important factor limiting the performance of the forecasted products was the accuracy of the weather model, as the underestimation of winds directly translates to underprediction of maximum water levels and wave heights. Lastly, the limited data availability for model setup and validation also hampered the assessment of the proposed framework. Our model validation process during both forecasted periods showed that the iFLOOD-Brazil model setup has the capability to reasonably provide real-time hydrodynamic and wave forecasts for the coastal areas of Southern Brazil.

This forecast system is a demonstration of technology capabilities applied to coastal communities in developing countries where limited data are available, such as in Brazil, providing flood condition information during extreme events. Additionally, the real-time forecasted products from iFLOOD are made freely available on a web-based data portal (https://iflood.vse.gmu.edu/) for general public use. Future work may focus on understanding the benefits of using a 3D baroclinic forecasting system to improve the hydrodynamic and wave forecasts within the study area.

Author Contributions: A.K. and A.d.S.d.L. designed the study. A.K. developed the operational framework and performed the analysis. The manuscript was written by A.K., A.d.S.d.L., F.C., T.M., and C.F. All authors have read and agreed to the published version of the manuscript.

Funding: This research was funded by Virginia Sea Grant College Program Project [R/72155C] grant number [NA18OAR4170083] from the National Oceanic and Atmospheric Administration's (NOAA) National Sea Grant College Program, U.S. Department of Commerce. The APC was funded by Virginia Sea Grant College Program Project grant [NA18OAR4170083] as well.

Acknowledgments: This publication was conducted using federal funds under the award number 204985, Virginia Sea Grant College Program Project (VASG Project# R/72155C), from the National Oceanic and Atmospheric Administration's (NOAA) National Sea Grant College Program, U.S. Department of Commerce. The research resources from the Flood Hazards Research Lab (FHRL) at George Mason University were also used to conduct this research. The authors also acknowledge the Santa Catarina Environmental Resources and Hydrometeorology Information Center (Epagri/CIRAM) regarding the oceanographic observational data used for model validation. Any opinions, findings, and conclusions or recommendations expressed in this material are those of the authors and do not necessarily reflect the views of the Virginia Sea Grant, NOAA, or the U.S. Department of Commerce. Additionally, this work used the Extreme Science and Engineering Discovery Environment (XSEDE) STAMPEDE2 resources through allocation id TG-BCS130009, which is supported by the National Science Foundation (grant number ACI- 1548562) [81]. The authors acknowledge the Texas Advanced Computing Center (TACC) at The University of Texas at Austin for providing HPC resources that contributed to the model calibration results reported within this paper (http://www.tacc.utexas.edu). This study was also financed in part by the Coordenação de Aperfeiçoamento de Pessoal de Nível Superior, Brasil (CAPES), finance code 001.

Conflicts of Interest: The authors declare no conflict of interest.

References

1. Zhou, L.; Hu, W.; Jia, Z.; Li, X.; Li, Y.; Su, T.; Guo, Q. Integrated visualization approach for real-time and dynamic assessment of storm surge disasters for China's seas. *ISPRS Int. J. Geo Inf.* **2020**, *9*, 51. [CrossRef]
2. Yin, K.; Xu, S.; Zhao, Q.; Huang, W.; Yang, K.; Guo, M. Effects of land cover change on atmospheric and storm surge modeling during typhoon event. *Ocean Eng.* **2020**, *199*. [CrossRef]
3. Rueda, A.; Camus, P.; Tomás, A.; Vitousek, S.; Méndez, F.J. A multivariate extreme wave and storm surge climate emulator based on weather patterns. *Ocean Model.* **2016**, *104*, 242–251. [CrossRef]
4. Lopes, C.L.; Dias, J.M. Assessment of flood hazard during extreme sea levels in a tidally dominated lagoon. *Nat. Hazards* **2015**, *77*, 1345–1364. [CrossRef]
5. Apollonio, C.; Bruno, M.F.; Iemmolo, G.; Molfetta, M.G.; Pellicani, R. Flood Risk Evaluation in Ungauged Coastal Areas. *Water* **2020**, *5*, 1466. [CrossRef]
6. Kim, S.; Pan, S.; Mase, H. Artificial neural network-based storm surge forecast model: Practical application to Sakai Minato, Japan. *Appl. Ocean Res.* **2019**, *91*, 101871. [CrossRef]
7. Rautenbach, C.; Williams, T.; De Vos, M.; Barnes, M.A. A coupled wave, tide and storm surge operational forecasting system for South Africa–Validation and physical description. *Nat. Hazards Submitt. Oct.* **2020**, *103*, 1407–1439. [CrossRef]

8. Costa, C.G.R.; Leite, J.R.B.; Castro, B.M.; Blumberg, A.F.; Georgas, N.; Dottori, M.; Jordi, A. An operational forecasting system for physical processes in the Santos-Sao Vicente-Bertioga Estuarine System, Southeast Brazil. *Ocean Dyn.* **2020**, *70*, 257–271. [CrossRef]
9. Lin, I.I.; Goni, G.J.; Knaff, J.A.; Forbes, C.; Ali, M.M. Ocean heat content for tropical cyclone intensity forecasting and its impact on storm surge. *Nat. Hazards* **2013**, *66*, 1481–1500. [CrossRef]
10. Lakshmi, D.D.; Murty, P.L.N.; Bhaskaran, P.K.; Sahoo, B.; Kumar, T.S.; Shenoi, S.S.C.; Srikanth, A.S. Performance of WRF-ARW winds on computed storm surge using hydodynamic model for Phailin and Hudhud cyclones. *Ocean Eng.* **2017**, *131*, 135–148. [CrossRef]
11. Altaf, M.U.; Butler, T.; Luo, X.; Dawson, C.; Mayo, T.; Hoteit, I. Improving short-range ensemble kalman storm surge forecasting using robust adaptive inflation. *Mon. Weather Rev.* **2013**, *141*, 2705–2720. [CrossRef]
12. Murty, P.L.N.; Srinivas, K.S.; Rao, E.P.R.; Bhaskaran, P.K.; Shenoi, S.S.C.; Padmanabham, J. Improved cyclonic wind fields over the Bay of Bengal and their application in storm surge and wave computations. *Appl. Ocean Res.* **2020**, *95*, 102048. [CrossRef]
13. Zhang, K.; Li, Y.; Liu, H.; Rhome, J.; Forbes, C. Transition of the coastal and estuarine storm tide model to an operational storm surge forecast model: A case study of the florida coast. *Weather Forecast.* **2013**, *28*, 1019–1037. [CrossRef]
14. Sahoo, B.; Bhaskaran, P.K. Prediction of storm surge and inundation using climatological datasets for the Indian coast using soft computing techniques. *Soft Comput.* **2019**, *23*, 12363–12383. [CrossRef]
15. Flowerdew, J.; Mylne, K.; Jones, C.; Titley, H. Extending the forecast range of the UK storm surge ensemble. *Q. J. R. Meteorol. Soc.* **2013**, *139*, 184–197. [CrossRef]
16. Fernández-Montblanc, T.; Vousdoukas, M.I.; Ciavola, P.; Voukouvalas, E.; Mentaschi, L.; Breyiannis, G.; Feyen, L.; Salamon, P. Towards robust pan-European storm surge forecasting. *Ocean Model.* **2019**, *133*, 129–144. [CrossRef]
17. Hasegawa, H.; Kohno, N.; Higaki, M.; Itoh, M. Upgrade of JMA's Storm Surge Prediction for the WMO Storm Surge Watch Scheme (SSWS). *Tech. Rev. RSMC Tokyo* **2017**, *19*, 1–9.
18. Yang, K.; Paramygin, V.A.; Sheng, Y.P. A Rapid Forecasting and Mapping System of Storm Surge and Coastal Flooding. *Weather Forecast.* **2020**, 1663–1681. [CrossRef]
19. Loftis, J.D.; Mitchell, M.; Schatt, D.; Forrest, D.R.; Wang, H.V.; Mayfield, D.; Stiles, W.A. Validating an Operational Flood Forecast Model Using Citizen Science in Hampton Roads, VA, USA. *J. Mar. Sci. Eng.* **2019**, *7*, 242. [CrossRef]
20. Dresback, K.M.; Fleming, J.G.; Blanton, B.O.; Kaiser, C.; Gourley, J.J.; Tromble, E.M.; Luettich, R.A.; Kolar, R.L.; Hong, Y.; Van Cooten, S.; et al. Skill assessment of a real-time forecast system utilizing a coupled hydrologic and coastal hydrodynamic model during Hurricane Irene (2011). *Cont. Shelf Res.* **2013**, *71*, 78–94. [CrossRef]
21. Akbar, M.; Aliabadi, S.; Patel, R.; Watts, M. A fully automated and integrated multi-scale forecasting scheme for emergency preparedness. *Environ. Model. Softw.* **2013**, *39*, 24–38. [CrossRef]
22. Khalid, A.; Ferreira, C. Advancing real-time flood prediction in large estuaries: iFLOOD a fully coupled surge-wave automated web-based guidance system. *Environ. Model. Softw.* **2020**, *131*, 104748. [CrossRef]
23. Suh, S.W.; Lee, H.Y.; Kim, H.J.; Fleming, J.G. An efficient early warning system for typhoon storm surge based on time-varying advisories by coupled ADCIRC and SWAN. *Ocean Dyn.* **2015**, *65*, 617–646. [CrossRef]
24. Freeman, J.; Velic, M.; Colberg, F.; Greenslade, D.; Divakaran, P.; Kepert, J. Development of a tropical storm surge prediction system for Australia. *J. Mar. Syst.* **2020**, *206*, 103317. [CrossRef]
25. Resio, D.T.; Irish, J.L. Tropical Cyclone Storm Surge Risk. *Curr. Clim. Chang. Rep.* **2015**, *1*, 74–84. [CrossRef]
26. Ohz, A.; Klein, A.H.F.; Franco, D. A Multiple Linear Regression-Based Approach for Storm Surge Prediction Along South Brazil Arthur. In *Climate Change, Hazards and Adaptation Options*; Springer International Publishing: New York, NY, USA, 2020; pp. 369–388. ISBN 978-3-030-37424-2.
27. Li, T.; Wang, F.; Hou, J.; Che, Z.; Dong, J. Validation of an operational forecasting system of sea dike risk in the southern Zhejiang, South China. *J. Oceanol. Limnol.* **2019**, *37*, 1929–1940. [CrossRef]
28. Gomes, G.; Da Silva, A.C. Nearshore wave analysis in the Brazilian Northeast based on observations and numerical models. *J. Oper. Oceanogr.* **2018**, *11*, 44–53. [CrossRef]
29. Dinápoli, M.G.; Simionato, C.G.; Moreira, D. Development and validation of a storm surge forecasting/hindcasting modelling system for the extensive Río de la Plata Estuary and its adjacent Continental Shelf. *Nat. Hazards* **2020**. [CrossRef]

30. Gramcianinov, C.B.; Hodges, K.I.; Camargo, R. The properties and genesis environments of South Atlantic cyclones. *Clim. Dyn.* **2019**, *53*, 4115–4140. [CrossRef]
31. Machado, A.A.; Calliari, L.J. Synoptic Systems Generators of Extreme Wind in Southern Brazil: Atmospheric Conditions and Consequences in the Coastal Zone. *J. Coast. Res.* **2016**, *75*, 1182–1186. [CrossRef]
32. Machado, A.A.; Calliari, L.J.; Melo, E.; Klein, A.H.F. Historical assessment of extreme coastal sea state conditions in southern Brazil and their relation to erosion episodes. *Panam. J. Aquat. Sci.* **2010**, *5*, 105–114.
33. Marengo, J.A.; Scarano, F.R.; Klein, A.F.; Souza, C.R.G.; Chou, S.C. *Impacto, Vulnerabilidade E Adaptação Das Cidades Costeiras Brasileiras Às Mudanças Climáticas: Relatório Especial do Painel Brasileiro de Mudanças Climáticas*; Painel Brasileiro de Mudanças Climáticas (PBMC): Rio de Janeiro, Brazil, 2016; ISBN 9788528503456.
34. Rudorff, F.; Bonetti, J. *Maré de Tempestade*; IHGSC/Cadernos Geográficos: Florianópolis, Brazil, 2015.
35. Cyriac, R.; Dietrich, J.C.; Fleming, J.G.; Blanton, B.O.; Kaiser, C.; Dawson, C.N.; Luettich, R.A. Variability in Coastal Flooding predictions due to forecast errors during Hurricane Arthur. *Coast. Eng.* **2018**, *137*, 59–78. [CrossRef]
36. Morsy, M.M.; Goodall, J.L.; O'Neil, G.L.; Sadler, J.M.; Voce, D.; Hassan, G.; Huxley, C. A cloud-based flood warning system for forecasting impacts to transportation infrastructure systems. *Environ. Model. Softw.* **2018**, *107*, 231–244. [CrossRef]
37. Pezzi, L.P.; Souza, R.B. De A Review on the Ocean-Atmosphere Interaction Processes in Regions of Strong Sea Surface Temperature Gradients of The South Atlantic Ocean Based on Observational Data. *Rev. Bras. Meteorol.* **2016**, *31*, 428–453. [CrossRef]
38. Yang, F.; Pan, H.L.; Krueger, S.K.; Moorthi, S.; Lord, S.J. Evaluation of the NCEP global forecast system at the ARM SGP site. *Mon. Weather Rev.* **2006**, *134*, 3668–3690. [CrossRef]
39. De Lima, A.d.S.; Khalid, A.; Miesse, T.; Cassalho, F.; Ferreira, C.; Scherer, M.E.G.; Bonetti, J. Hydrodynamic and waves response during storm surges on the Southern Brazilian coast: A hindcast study. *Water* **2020**.
40. Rodríguez, M.G.; Nicolodi, J.L.; Gutiérrez, O.Q.; Losada, V.C.; Hermosa, A.E. Brazilian coastal processes: Wind, wave climate and sea level. In *Brazilian Beach Systems*; Short, A.D., Klein, A.H., Da, F., Eds.; Springer International Publishing: New York, NY, USA, 2016; pp. 37–66. ISBN 978-3-319-30392-5.
41. Sutil, U.A.; Pezzi, L.P.; De Cássia, R.; Alves, M.; Nunes, A.B. Anuário do Instituto de Geociências—UFRJ Ocean-Atmosphere Interactions in an Extratropical Cyclone in the Southwest Atlantic. *Anuário do Inst. Geociências—UFRJ* **2019**, *42*, 525–535. [CrossRef]
42. Campos, R.M.; Guedes Soares, C.; Alves, J.H.G.M.; Parente, C.E.; Guimaraes, L.G. Regional long-term extreme wave analysis using hindcast data from the South Atlantic Ocean. *Ocean Eng.* **2019**, *179*, 202–212. [CrossRef]
43. Dietrich, J.C.; Zijlema, M.; Westerink, J.J.; Holthuijsen, L.H.; Dawson, C.; Luettich, R.A.; Jensen, R.E.; Smith, J.M.; Stelling, G.S.; Stone, G.W. Modeling hurricane waves and storm surge using integrally-coupled, scalable computations. *Coast. Eng.* **2011**, *58*, 45–65. [CrossRef]
44. Luettich, R.A.; Westerink, J.J.; Scheffner, N.W. ADCIRC: An advanced three-dimensional circulation model for shelves, coasts, and estuaries. Report 1. In *Theory and Methodology of ADCIRC-2DDI and ADCIRC-3DL*; Coastal Engineering Research Center: Vicksburg, MS, USA, 1992.
45. Booij, N.; Ris, R.C.; Holthuijsen, L.H. A third-generation wave model for coastal regions. *J. Geophical Res.* **1999**, *104*, 7649–7666. [CrossRef]
46. Blain, C.A.; Linzell, R.S.; Chu, P.; Massey, C. *Validation test report for the ADvanced CIRCulation Model (ADCIRC) v45. 11*; DTIC Document: Fort Belvoir, VA, USA, 2010.
47. Garzon, J.L.; Ferreira, C.M.; Padilla-Hernandez, R. Evaluation of weather forecast systems for storm surge modeling in the Chesapeake Bay. *Ocean Dyn.* **2018**, *68*, 91–107. [CrossRef]
48. Hanson, J.; Wadman, H.; Blanton, B.; Roberts, H. *ERDC/CHL TR-11-1 Coastal Storm Surge Analysis: Modeling System Validation*; Report 4: Intermediate Submission No. 2.0; The US Army Engineer Research and Development Center (ERDC): Kitty Hawk, NC, USA, 2013.
49. Shen, J.; Wang, H.; Sisson, M.; Gong, W. Storm tide simulation in the Chesapeake Bay using an unstructured grid model. *Estuar. Coast. Shelf Sci.* **2006**, *68*, 1–16. [CrossRef]
50. Fleming, J.G.; Fulcher, C.W.; Luettich, R.A.; Estrade, B.D.; Allen, G.D.; Winer, H.S. A real time storm surge forecasting system using ADCIRC. In Proceedings of the International Conference on Estuarine and Coastal Modeling, Newport, RI, USA, 5–7 November 2007; pp. 893–912.

51. Funakoshi, Y.; Feyen, J.; Aikman, F.; Tolman, H.; Van Der Westhuysen, A.; Chawla, A.; Rivin, I.; Taylor, A. Development of extratropical surge and tide operational forecast system (ESTOFS). In Proceedings of the International Conference on Estuarine and Coastal Modeling, Augustine, FL, USA, 7–9 November 2011; pp. 201–212.
52. Mattocks, C.; Forbes, C. A real-time, event-triggered storm surge forecasting system for the state of North Carolina. *Ocean Model.* **2008**, *25*, 95–119. [CrossRef]
53. Roberts, K.J.; Pringle, W.J.; Westerink, J.J. OceanMesh2D 1.0: MATLAB-based software for two-dimensional unstructured mesh generation in coastal ocean modeling. *Geosci. Model Dev.* **2019**, *12*, 1847–1868. [CrossRef]
54. Wessel, P.; Smith, W.H.F. A global, self-consistent, hierarchical, high-resolution shoreline database. *J. Geophys. Res. Solid Earth* **1996**, *101*, 8741–8743. [CrossRef]
55. GEBCO. *Compilation Group General Bathymetric Chart of the Oceans*; British Oceanographic Data Centre: Liverpool, UK, 2019.
56. Quetzalcóatl, O.; González, M.; Cánovas, V.; Medina, R.; Espejo, A.; Klein, A.; Tessler, M.G.; Almeida, L.R.; Jaramillo, C.; Garnier, R.; et al. SMCε, a coastal modeling system for assessing beach processes and coastal interventions: Application to the Brazilian coast. *Environ. Model. Softw.* **2019**, *116*, 131–152. [CrossRef]
57. Egbert, G.D.; Erofeeva, S.Y. Efficient Inverse Modeling of Barotropic Ocean Tides. *J. Atmos. Ocean. Technol.* **2002**, *19*, 183–204. [CrossRef]
58. Atkinson, J.; Ph, D.; Hagen, S.C.; Ce, D.; Wre, D.; Zou, S.; Bacopoulos, P.; Medeiros, S.; Weishampel, J. Deriving Frictional Parameters and Performing Historical Validation for an ADCIRC Storm Surge Model of the Florida Gulf Coast. *Fla. Watershed* **2011**, *4*, 22–27.
59. Garzon, J.L.; Ferreira, C.M. Storm surge modeling in large estuaries: Sensitivity analyses to parameters and physical processes in the Chesapeake Bay. *J. Mar. Sci. Eng.* **2016**, *4*, 45. [CrossRef]
60. Tolman, H.L. The numerical model WAVEWATCH. No. 1989 02. *Commun. Hydraul. Geotech. Eng.* **1989**.
61. Manganello, J.V.; Hodges, K.I.; Kinter, J.L.; Cash, B.A.; Marx, L.; Jung, T.; Achuthavarier, D.; Adams, J.M.; Altshuler, E.L.; Huang, B.; et al. Tropical cyclone climatology in a 10-km global atmospheric GCM: Toward weather-resolving climate modeling. *J. Clim.* **2012**, *25*, 3867–3893. [CrossRef]
62. Liu, H.; Taylor, A. Development of the nws' probabilistic extra-tropical storm surge model and post processing methodology. In Proceedings of the 98th AMS Annual Meeting, Austin, TX, USA, 7–11 January 2018.
63. Gobato, R.; Heidari, A. Cyclone Bomb hits Southern Brazil in 2020. *J. Atmos. Sci. Res.* **2020**, *3*, 8–12. [CrossRef]
64. Hodges, K.I.; Lee, R.W.; Bengtsson, L. A comparison of extratropical cyclones in recent reanalyses ERA-Interim, NASA MERRA, NCEP CFSR, and JRA-25. *J. Clim.* **2011**, *24*, 4888–4906. [CrossRef]
65. Stopa, J.E.; Cheung, K.F. Periodicity and patterns of ocean wind and wave climate. *J. Geophys. Res. Ocean.* **2014**, *119*, 2227–2237. [CrossRef]
66. Franz, G.A.S.; Leitão, P.; Dos Santos, A.; Juliano, M.; Neves, R. From regional to local scale modelling on the south-eastern Brazilian shelf: Case study of Paranaguá estuarine system. *Braz. J. Oceanogr.* **2016**, *64*, 277–294. [CrossRef]
67. Torres, M.J.; Hashemi, M.R.; Hayward, S.; Spaulding, M.; Ginis, I.; Grilli, S.T. Role of hurricane wind models in accurate simulation of storm surge and waves. *J. Waterw. Port Coast. Ocean Eng.* **2019**, *145*. [CrossRef]
68. Choi, B.H.; Kim, K.O.; Yuk, J.-H.; Lee, H.S. Simulation of the 1953 storm surge in the North Sea. *Ocean Dyn.* **2018**, *68*, 1759–1777. [CrossRef]
69. Mayo, T.; Lin, N. The effect of the surface wind field representation in the operational storm surge model of the National Hurricane Center. *Atmosphere* **2019**, *10*, 193. [CrossRef]
70. Daines, J.T.; Monahan, A.H.; Curry, C.L. Model-based projections and uncertainties of near-surface wind climate in western Canada. *J. Appl. Meteorol. Climatol.* **2016**, *55*, 2229–2245. [CrossRef]
71. Kim, S.-C.; Chen, J.; Shaffer, W.A. An operational forecast model for extratropical storm surges along the US east coast. In *Preprints Conference on Coastal Oceanic and Atmospheric Prediction*; NOAA: Silver Springs, MD, USA, 1996; pp. 281–286.
72. Lanerolle, L.W.J.; Patchen, R.C.; Aikman, F., III. The second generation chesapeake bay operational forecast system (CBOFS2): A ROMS-based modeling system. In Proceedings of the Estuarine and Coastal Modeling, Seattle, WA, USA, 4–6 November 2009; American Society of Civil Engineers: Reston, VA, USA; pp. 621–642.
73. Weisberg, R.H.; Zheng, L. Hurricane storm surge simulations comparing three-dimensional with two-dimensional formulations based on an Ivan-like storm over the Tampa Bay, Florida region. *J. Geophys. Res. Ocean.* **2008**, *113*, 1–17. [CrossRef]

74. Weaver, R.; Luettich, R. 2D vs. 3D storm surge sensitivity in ADCIRC: Case study of hurricane Isabel. In Proceedings of the Estuarine and Coastal Modeling, Seattle, WA, USA, 4–6 November 2009; pp. 762–778.
75. Sheng, Y.P.; Alymov, V.; Paramygin, V.A. Simulation of storm surge, wave, currents, and inundation in the outer banks and Chesapeake bay during Hurricane Isabel in 2003: The importance of waves. *J. Geophys. Res. Ocean.* **2010**, *115*. [CrossRef]
76. Orton, P.; Georgas, N.; Blumberg, A.; Pullen, J. Detailed modeling of recent severe storm tides in estuaries of the New York City region. *J. Geophys. Res. Ocean.* **2012**, *117*. [CrossRef]
77. Marsooli, R.; Orton, P.M.; Mellor, G.; Georgas, N.; Blumberg, A.F. A coupled circulation-wave model for numerical simulation of storm tides and waves. *J. Atmos. Ocean. Technol.* **2017**, *34*, 1449–1467. [CrossRef]
78. Zheng, L.; Weisberg, R.H.; Huang, Y.; Luettich, R.A.; Westerink, J.J.; Kerr, P.C.; Donahue, A.S.; Crane, G.; Akli, L. Implications from the comparisons between two- and three-dimensional model simulations of the Hurricane Ike storm surge. *J. Geophys. Res. Ocean.* **2013**, *118*, 3350–3369. [CrossRef]
79. Janssen, P.A.E.M.; Bidlot, J.R. Progress in operational wave forecasting. In *Proceedings of the IUTAM Symposium Wind Waves*; Elsevier B.V.: London, UK, 2017; pp. 14–29.
80. Li, J.; Zhang, S. Mitigation of model bias influences on wave data assimilation with multiple assimilation systems using WaveWatch III v5.16 and SWAN v41.20. *Geosci. Model Dev.* **2020**, *13*, 1035–1054. [CrossRef]
81. Towns, J.; Cockerill, T.; Dahan, M.; Foster, I.; Gaither, K.; Grimshaw, A.; Hazlewood, V.; Lathrop, S.; Lifka, D.; Peterson, G.D.; et al. XSEDE: Accelerating scientific discovery. *Comput. Sci. Eng.* **2014**, *16*, 62–74. [CrossRef]